Title: Structural Variants of Biodegradable Polyesterurethane *In-Vivo* Evoke a Cellular and Angiogenic Response that is Dictated by Architecture

Authors: Jerome A. Henry[1,2], Krishna Burugapalli[1,2], Peter Neuenschwander[3], Abhay Pandit[1,2,*]

Affiliations: [1]Department of Mechanical and Biomedical Engineering, National University of Ireland, Galway, Galway, Ireland

[2]National Centre for Biomedical Engineering Science, National University of Ireland, Galway, Galway, Ireland

[3]Polymer Technology, Department of Materials, ETH Zurich, Zurich 8093, Switzerland

* To whom correspondence and reprint requests should be addressed: Department of Mechanical and Biomedical Engineering, National University of Ireland, Galway, University Road, Galway, Ireland.

E-mail: Abhay.Pandit@nuigalway.ie

Phone: +353 91 492758

Fax: +353 91 563991

Abstract

The aim of this study was to investigate an *in-vivo* tissue response to a biodegradable polyesterurethane, specifically the cellular and angiogenic response evoked by varying implant architectures in a subcutaneous rabbit implant model. A synthetic biodegradable polyesterurethane was synthesised and processed into three different configurations; a non-porous film, a porous mesh and a porous membrane. Glutaraldehyde cross-linked bovine pericardium was used as a control. Sterile polyesterurethane and control samples were implanted subcutaneously in six rabbits, (n=12). The rabbits were sacrificed at 21 and 63 days and the implant sites were sectioned and histologically stained using haemotoxylin and eosin (H&E), Masson's trichrome, picosirius red and immunostain CD31. The tissue-implant interface thickness was measured from the H&E slides. Stereological techniques were used to quantify the tissue reaction at each time point that included volume fraction of inflammatory cells, fibroblasts, fibrocytes, collagen and the degree of vascularisation. Stereological analysis inferred that porous scaffolds with regular topography are better tolerated in-vivo compared to non-porous scaffolds, while increasing scaffold porosity promotes angiogenesis and cellular infiltration. The results suggest that this biodegradable polyesterurethane is better tolerated *in-vivo* than the control and that structural variants of biodegradable polyesterurethane *in-vivo* evoke a cellular and angiogenic response that is dictated by architecture.

Keywords: polyesterurethane, tissue response, scaffold

1. Introduction

Synthetic biodegradable polymers are becoming increasingly popular for clinical and surgical applications as it is possible to control their mechanical properties and degradation rates, depending on the particular application. Furthermore, these polymers may be processed into a variety of porous and non-porous structures, using processes such as rapid-prototyping, electrospinning, freeze drying, phase inversion and solvent casting [1,2]. The degree of tissue infiltration can be controlled by the morphology and porosity of the scaffold [3]. The porous architecture of the former allows the cells to penetrate the structure thus increasing the surface area where they can proliferate.

Implant architecture is known to influence the inflammatory and angiogenic response *in-vivo*. Rough implant architectures have been reported to evoke a greater macrophage response and induce greater numbers of giant cells compared to smooth implant surfaces [4-6]. Electrospun meshes with a fibre diameter less than 10µm were shown to be less susceptible to encapsulation compared to meshes with a fibre diameter greater than 10µm [7,8]. It was also noted that electrospun meshes with an inter-fibre distance smaller than 100µm, experience less tissue infiltration and greater encapsulation compared to meshes with an inter-fibre distance larger than 100µm [7,8]. The interstitial inter-fibre distance is determinant with regards to the degree of angiogenesis within a porous implant, as arterioles have a diameter of 30-500µm [9]. Furthermore, implant architecture affects the degradation rate of biodegradable polymers, since porous scaffolds have a larger surface area in contact with fluids than non-porous scaffolds.

Biodegradable polyesterurethanes have been investigated *in-vitro* and *in-vivo* for various tissue-engineering applications [1,3,10-12]. A slowly degrading polyesterurethane

with a crystalline segment of poly((R)-3-hydroxybutyric acid)-diol linked with a diisocyanate to an amorphous segment of poly(ε-caprolactone-*co*-glycolide)-diol has been developed [13]. The ratio of the soft to hard segments has been based on a predicted long-term degradation period having considered preceding data on DegraPol™ which indicated the degradation rate and the respective stoichiometric ratios of the crystalline to amorphous segments [11,14,15]. Our earlier study characterised and reported the *in-vitro* behaviour of this polymer with respect to change in mechanical properties, molecular weight and cell viability [13]. This is the first study to characterise the *in-vivo* response of this specific blend of polyesterurethane.

The aim of this study was to investigate the cellular and angiogenic response evoked by varying implant architectures in a subcutaneous rabbit implant model at 21 and 63 days. In this study, three scaffolds were processed from the same polyesterurethane; a non-porous film using solvent casting, an electrospun porous mesh and a porous membrane fabricated by a phase inversion method. The control was bovine pericardium. Haemotoxylin and Eosin (H&E) and Masson's trichrome stains were used to assess the tissue response at both time points for all four variants. Picosirius red stain and polarised light microscopy were used to examine collagen orientation around the four implants. Immunostain CD31 highlighted endothelial cells to later quantify angiogenesis. Stereological techniques quantified the tissue-implant interface thickness, the volume fraction of inflammatory cells, fibroblasts, fibrocytes, collagen and degree of angiogenesis specific to each scaffold.

2. Materials and methods

2.1 Polymer synthesis

A biodegradable polyesterurethane polymer with poly(hydroxybutyrate) for the crystalline segment and diglycolide and ε-caprolactone for the amorphous segments was used in this study [13]. The stoichiometric ratio of the crystalline to amorphous segments was 1:1.5 respectively. The crystalline and amorphous segments were cross-linked with 2, 2, 4-trimethyl hexamethylene diisocyanate (TMDI). Throughout the synthesis, Fourier transform infrared (FTIR) (Bruker Vertex 70, Bruker Optics GmbH, Faellanden, Switzerland) measurements were taken at regular intervals to identify the presence of the unreacted cross-linker TMDI (-NCO) groups at 2250 cm^{-1}. When the FTIR spectra no longer detected the TMDI, the polymer synthesis was considered complete. The polymer synthesis was concluded after 120h. Subsequently, the synthesised polymer was precipitated into -70°C methanol to prevent premature hydrolysis. Following precipitation, the polymer was vacuum-filtered to remove excess solvent and later dried in a vacuum oven at -10mBar for 72h prior to processing.

2.2 Scaffold manufacture

2.2.1 Fabrication of film

A 20% (w/w) polymer solution was prepared in chloroform (Merck KgaA, Germany) [13]. The solution was cast using a 500µm doctor's blade on a polytetrafluoroethylene-coated plate. The wet films were left under a fume hood to allow solvent evaporation.

2.2.2 Fabrication of mesh

A 27% (w/w) polymer solution was dissolved in chloroform [13]. 10ml of the solution was extracted with a syringe and secured in a syringe pump (Aladdin-220 Programmable Syringe Pump, World Precision Instruments, Stevenage, UK). A cooled cylindrical target at -70°C was positioned 200mm away from the needle. A high voltage supply (Glassman Europe Ltd, UK) was attached to the needle. The target was rotated at 300rpm, the syringe flow-rate was 4ml/h, with the high voltage supply 18kV. The processing time was 2.5h. The processed electrospun mesh was removed from the target and stored in a vacuum chamber to remove excess solvent and moisture accumulated during processing.

2.2.3 Fabrication of membrane

A 15% (w/w) solution was dissolved in 1, 4-dioxane, this concentration determined from previous studies, and cast into a wet film using a 500µm doctor's blade. This film was immersed in containers of methanol and ethanol for five minutes each. Finally, the glass plate and membrane were then transferred to a container of distilled water for five minutes. The immersion of the film in the non-solvents created a porous membrane. The porous membranes were stored in a vacuum chamber to remove excess moisture.

2.2.4 Control

Glutaraldehyde treated bovine pericardium (Peri-Strip®, Biovascular Inc., Saint Paul, MN) was used as a control, as this is FDA-approved for reinforcing surgical staples. This biomaterial also has a long degradation rate but must be pre-treated for enhanced

mechanical properties and degradation rate. Hence a slowly degrading polyesterurethane that requires no pretreatment prior to processing may be an alternative.

2.3 Scaffold sterilisation

All polymer scaffolds were sterilised with ethylene oxide prior to implantation. The control was supplied sterilised.

2.4 Scaffold characterisation

Sterilised and nonsterilised polyesterurethane scaffold morphology was examined with scanning electron microscopy (SEM). Scaffolds were sputter coated with gold prior to SEM examination (Hitachi Field Emission Scanning Electron Microscope). Pore size and filament diameter of the processed mesh and membrane scaffolds were quantified from the SEM images. Mean film and control thicknesses were determined using a micrometer from four random thickness measurements.

SEM images of the electrospun mesh were exported to an image analysis software program (Image Pro® Plus, Media Cybernetics, UK) to obtain Fast Fourier Transform (FFT) algorithms. For every radial angle from the centre of the FFT image, the software adds together the intensities of all the points found within one degree. The ratios between the total FFT intensities for every angle indicate the ratios at which lines can be found at different angles in the original SEM pictures. The location and intensity of all the points in the FFT results were stored in an EXCEL® spreadsheet. A method for transforming FFT visual outputs into numerical data was developed and automated through a custom-made software. The following parameters were quantified: fibre orientation, porosity,

pore size and pore aspect ratio. The pore distribution was calculated for pore sizes between 10µm and 200µm.

2.5 Subcutaneous implantation

Six white New Zealand male rabbits weighing between 2.8 and 3.0kg were used in this study. All animals were housed singly and had access to standard pellet diet and water *ad libitum*. Ethical approval for the procedures was obtained from the Institutional Animal Ethics Committee of the National University of Ireland, Galway. The study was covered under a license issued by the Department of Health and Children, Government of Ireland, licence reference B100/3316. The rabbits were acclimatised to local environment for one week prior to surgery.

The rabbits were anaesthesised using ketamine (100mg/kg IM) and xylazine (5mg/kg IM) (Narketan and Xylapan, Vetoquinol Ltd., UK). The backs of the anaesthesised rabbits were clipped and subsequently cleaned with iodine. A total of eight transverse incisions, four each on either side of the dorsal midline, were made on the back of the rabbit. Each incision was separated from the other by at least 5cm. At each incision a subcutaneous pocket was made towards the anterior side (neck) of the rabbit. One 10x10 mm sterile scaffold was secured in each subcutaneous pocket using two stitches with a non-absorbable suture (Ethicon™ 4-0 Prolene®, Johnson & Johnson Ireland Ltd., Dublin), in corners of the scaffold. Following implantation, the incisions were closed with an absorbable polyester suture (Ethicon™ 4-0 Vicryl®, Johnson & Johnson Ireland Ltd., Dublin).

The six rabbits were divided into two groups of three each. Each rabbit received eight implants and the positioning of the implants on the back of the rabbit was randomised and recorded. Four scaffold variants (film, membrane and mesh configurations of the polyurethane, and bovine pericardium as control) were investigated in this study. The two groups of rabbits were sacrificed at 21 and 63 days with an overdose of sodium pentobarbitone. There were a total of six treatments per scaffold variant per time point. At the time of sacrifice, the implant sites (overlying skin, implant, surrounding tissue and underlying subcutaneous muscle) were retrieved and fixed in 10% neutral buffered formalin.

2.6 Histopathology and staining

The formalin fixed tissues were dehydrated and permeated with paraffin in automatic tissue processor (Leica ASP300), blocked (LeicaEG1150H and EG1150C) in paraffin and sectioned (Leica RM2235) perpendicular to the skin surface in 5µm sections. The slides were stained with haematoxylin & eosin (H&E), Masson's trichrome (MT), picosirius red and immunostain CD31 for subsequent stereological analysis.

H&E and MT staining kits (Cat. No. 631200 and 631065 respectively, Clin-Tech Ltd., Surrey, UK) were used for H&E and MT staining in accordance to manufacturer recommended protocol. For picosirius red staining, paraffin sections were deparaffinised twice in xylene, five minutes each, followed by dehydration in 100%, 95% and 70% ethanol and running tap water for two minutes each. The slides were then rinsed in distilled water twice, two minutes each and subsequently covered in picosirius red stain (Sircol Collagen Assay Dye, Biocolor Ltd., Northern Ireland) for 1h. Following staining,

the slides were washed twice with 0.1M HCl in distilled water, two minutes each. The sections were dehydrated through 70%, 95% and 100% ethanol, cleared in two changes of xylene and mounted with dibutyl phthalate xylene (DPX).

CD31 is expressed by endothelial cells; hence CD31 labelled cells would detect angiogenesis [19,20]. Paraffin sections were stained for CD31 using a blood vessel staining kit (ECM590, Millipore Ireland, Carrigtwohill, Ireland) according to the protocol recommended for the kit, except that the primary antibody used was monoclonal mouse anti human CD31 (Dako, Germany) at 1:40 solution in primary dilution buffer. For antigen retrieval, microwave processing at 98^{o}C for 30 minutes in tris base buffer (10mM tris base, 1 mM ethylene diamine tetra acetic acid, 0.05% Tween 20, pH 9.0) was used. Mayer's haematoxylin was used as the counter stain. The immunohistochemical stained sections were subsequently dehydrated through 70%, 95% and 100% ethanol, cleared in two changes of xylene and mounted with DPX.

The stained sections were observed under a light microscope fitted with a digital camera (Olympus BX51, DP-70 digital camera, Mason Technology, Dublin). For polarised light microscopy, simple polariser-analyser accessories (Olympus U-POT simple polariser, U-ANT analyser oriented orthogonal to the polarised beam and 530nm filter for bifringence, Mason Technology, Dublin) were used to characterise the picosirius red stained collagen fibres, which appeared as red, yellow and green. Red and yellow were denoted collagen type I-like whilst green was denoted collagen type III-like [16-18]. Digital images for stereological analysis were captured using image analysis software (Image Pro® Plus, Media Cybernetics, UK).

2.7 Quantitative histological analysis

2.7.1 Stereological analysis

Stereological quantification of the histopathological images was based on the methods described by Garcia et al [21]. The extracellular matrix deposition (for tissue composition), inflammatory cell distribution in the implant area (cellular composition) and angiogenesis were quantified in this study. The minimal number of fields of view per slide had been estimated in a previous pilot study. Six random representative images were taken on each slide at x100 magnification using the imaging analysis software. A rectangular grid containing 108 square grids, each with an area of $1.0x10^{-4}mm^2$, was superimposed on each image.

2.7.2 Tissue composition

The volume fraction of extracellular (collagenous) matrix deposition, inflammatory cells and angiogenesis was determined from the Masson's trichrome stained slides. In the case of the mesh, the ratio of tissue infiltration to implant was expressed as a percentage of the total sampling area at 21 days and 63 days. This ratio gave an indirect indication to the degree of scaffold degradation from 21 days to 63 days.

2.7.3 Cellular response

The H&E stained slides were used to identify and quantify the inflammatory cell response in the tissue-implant interface and reaction zone by calculating the volume fractions of lymphocytes, plasma cells, fibroblasts, fibrocytes and giant cells. Cells such as neutrophils and macrophages were grouped as mononuclear cells.

2.7.4 Angiogenesis

Capillaries provide the means for exchanging blood, oxygen, nutrients and waste products to the newly formed tissue. Hence it is critical to understand the degree of angiogenesis occurring within and around the degrading scaffolds. Angiogenesis was quantified from the CD31 stained slides using a cycloid grid [21]. Specifically, the capillary length density, L_v, capillary surface area density, S_v and radial diffusion difference, R_{diff}, were measured.

2.8 Statistical analysis

Statistical analyses were carried out using statistical software (Minitab™, v.13.32). Statistical variances between groups were determined by one way analysis of variance (ANOVA). Tukey's honestly significant difference test was used for *post hoc* evaluation of differences between groups. A p value of <0.05 was considered to be statistically significant.

3. Results

3.1 Scaffold characterisation

All polyesterurethane scaffolds morphologies were examined with SEM. There were no morphological differences between sterilised and nonsterilised architectures. The films had a non-porous morphology (Figure 1(a)). Film thickness was measured to be 111±9μm. The porous membrane morphology was also consistent, as per Figure 1(b),

with pore size 17±7μm. SEM examination of the electrospun meshes confirmed a homogenous structure, with consistent filament diameter, as seen in Figure 1(c). Fibre diameter was 10±2μm, while the inter-fibre distance was 107±58μm. The control had a thickness of 454 ±42μm.

The fibre orientation of the electrospun mesh was seen to be randomly distributed (data not shown). There was no statistical difference between any of the groups. Quantitative analysis of the mesh porosity, pore size and pore aspect ratio is shown in Table 1.

3.2 Subcutaneous implantation

All animals made a normal recovery after surgery. There were no obvious signs of degradation, such as scaffold cracking or scaffold disintegration for the three polyesterurethane implants at 21 days or 63 days. Histologically stained cross-sections of the film confirmed a non-porous scaffold, as shown in Figure 2(a, b). The mesh had superior pore interconnectivity compared to the membrane and control, as evident from Figure 2(c - h). Furthermore, there were no signs of adverse reaction with the implants such as swelling, ulceration, discharge of pus, scarring, tissue necrosis or avascular fibrous capsule formation at both 21 days and 63 days.

From the histological images, there were two layers evident around the film, membrane and control implants, as shown in Figure 2(a-f). The inner layer was a thin layer which was densely populated with cell nuclei. This layer was denoted the tissue-implant interface. The tissue-implant interface is the inflammatory response evoked by a foreign material when placed *in-vivo*. The tissue-implant interface thickness is inversely

related to how well an implanted material is tolerated by the host tissue, i.e. the thicker the interface the less well tolerated the material. Over time the tissue-implant interface is replaced by granulation tissue. There was no tissue-implant interface evident around the mesh samples, as seen in Figure 2(g, h). This absence of interface was due to tissue infiltration. An outer layer was evident around all four implants. This layer was considered as the "reaction zone".

Using the electronic callipers on the image analysis software (Image Pro® Plus, Media Cybernetics, UK), six representative tissue-implant interface thickness measurements were taken on each image. The tissue-implant interface thickness was measured for both time points, as shown in Table 2. At 21 days, the tissue-implant interface thickness was maximal for the control and minimal for the mesh. The interface thickness of the control was statistically different ($p<0.05$) to the three polyesterurethane constructs at both time points. There was no statistical difference between the film and membrane values, but the interface thickness at the mesh was statistically lower ($p<0.05$) to these two scaffolds at both time points.

3.3 Quantitative analysis

3.3.1 Tissue composition

Tissue-implant interface. The film, membrane and control samples were surrounded by a tissue-implant interface. There was no tissue-implant interface surrounding the mesh. Stereological volume fraction analysis of the extracellular (collagenous) matrix deposition, inflammatory cells and angiogenesis is shown in Figure 3(a). The quantity of collagenous tissue detectable within the tissue-implant interface at both time points was

negligible for all scaffolds. There were larger quantities of inflammatory cells present in the tissue implant interface around the film and membrane compared to the control at 21 days. From 21 days to 63 days, there was an increase in inflammatory cells around the film, membrane and control within the tissue-implant interface. There was no significant change in the magnitude of angiogenesis within the tissue-implant interface of the film, membrane and control constructs at both 21 days and 63 days.

Reaction zone. The volume fractions of extracellular (collagenous) matrix deposition, inflammatory cells and angiogenesis within the reaction zone which was present around all four implants, are shown in Figure 3(b). There was an increase in the volume fraction of collagenous tissue in the reaction zone around all three polyesterurethane scaffolds, significantly in the case of the membrane, (p<0.05). Conversely, there was a decrease in collagenous tissue within the control reaction zone. At 21 days, there was a significant difference between the volume fraction of film and mesh inflammatory cells, (p<0.05), while at 63 days, the control had prevalent inflammatory cells out of the four scaffolds. There was an increase in the volume fraction of angiogenesis for all four implants from 21 days to 63 days, although not significant.

Cellular infiltration into the mesh scaffold was visible at both 21 days and 63 days. The volume fraction of the histological response, angiogenesis and implant material was quantified, as shown in Figure 3(c). Within the mesh, there was a decrease in the degree of angiogenesis from 21 days to 63 days. The volume fraction of inflammatory cells significantly decreased after 63 days, (p<0.05). Although not significant, there was a decrease in the volume fraction of polymer from 21 days to 63 days. No collagenous tissue was detectable within the mesh at either time point.

Using the polarised light, collagen type I-like (red and yellow) and collagen type III-like fibres (green) were seen parallel to the implants, as in Figure 4. There was no collagen present within the film, mesh or membrane at either time point, Figure 4(a-f). Conversely, there was both collagen type I-like and collagen type III-like collagen within the control at 21 days and 63 days, Figure 4(g, h).

3.3.2 Cellular response

Tissue-implant interface. The cellular response within the tissue-implant interface was quantified and is shown in Figure 5(a). There were no discernable giant cells (GC) in the interfaces of the film, membrane and control at 21 days, but they were detectable at 63 days, with a significantly larger amount of giant cells around the membrane, ($p<0.05$). The film, membrane and control scaffold tissue-implant interfaces had decreased amounts of lymphocytes (L) from 21 days to 63 days. This decrease was significant for the film and membrane, ($p<0.05$). The control interface had greater amounts of lymphocytes at 63 days compared to the film and membrane. There was a significant increase in the volume fraction of fibroblasts (Fb) in the film, membrane and control tissue-implant interface from 21 days to 63 days, ($p<0.05$). No fibrocytes (Fc) were present at either time point in the tissue-implant interface of the film, membrane and control scaffolds. There were plasma cells (P) present at 21 days around the constructs, but the plasma cells were not detectable at 63 days. The volume fraction of mononuclear cells (MN) in the film, membrane and control tissue-implant interfaces from 21 days to 63 days decreased; significantly in the case of the control, ($p<0.05$).

Reaction zone. The inflammatory cell response within the reaction zone was analysed using stereological methods. The response is illustrated in Figure 5(b). There were no giant cells seen in the reaction zone of the four variants at both time points. All four variants recorded a decrease in the volume fraction of lymphocytes (L) from 21 days to 63 days. This decrease was significant for the film, mesh and membrane, (p<0.05). Furthermore, the control reaction zone consistently had the largest volume fraction of lymphocytes within the reaction zone at both time points. All four scaffolds had increased fibroblasts (Fb) volume fractions from 21 days to 63 days, significantly for the film, membrane and control, (p<0.05). There was an increase in the volume fraction of fibrocytes (Fc) for the film, membrane and control from 21 days to 63 days, significantly so in the case of the control (p<0.05). Conversely, there was a decrease in the volume fraction of fibrocytes within the mesh reaction zone. No plasma cells (P) were detectable in the reaction zone of all four implants at 63 days, representing a significant decrease from 21 days, (p<0.05). There was a decrease in the volume fraction of other mononuclear cells (MN) for all four implants, significantly in the case of the film, mesh and control, (p<0.05). Indeed, there were no mononuclear cells detectable for the film and mesh at 63 days.

The inflammatory cell response within the mesh is quantified in Figure 5(c). Giant cells were not present in the 21 days tissue infiltration, but there was a significant increase at 63 days, (p<0.05). The volume fraction of lymphocytes significantly decreased from 21 days to 63 days, (p<0.05). There was a significant decrease in the volume fraction of fibroblasts (p<0.05) from 21 days to 63 days, with no detectable fibrocytes at either time point. Plasma cells were not present at 63 days, representing a

significant decrease from 21 days, (p<0.05). There was a non-significant decrease in other mononuclear cells from 21 days to 63 days.

3.3.3 Angiogenesis

Immunohistochemistry staining for CD31 detected endothelial cells which inferred angiogenesis within the tissue-implant interface and reaction zone of all four implants, as in Figure 6. No endothelial cells were detected within the porous scaffolds except for the mesh, Figure 6(c).

Tissue-implant interface. There was an increase in the L_v (data not shown) and S_v (Figure 7(a)) for the film and membrane from 21 days to 63 days, while these two parameters decreased for the control. The membrane tissue-implant interface had the highest S_v at 63 days. There was a reduction in the R_{diff} for the film, mesh and control from 21 days to 63 days (Figure 7(b)); significantly so for the film, (p<0.05). As seen in Figure 7(b), R_{diff} was maximal for the membrane and minimal for the film at 63 days.

Reaction zone. The three polyesterurethane scaffolds had decreased L_v from 21 days to 63 days, while the control L_v increased by almost a factor of three (p<0.05). The S_v within the reaction zone of the four scaffolds is shown in Figure 8. The film S_v decreased by 3% from 21 days to 63 days while the membrane and mesh S_v decreased by 56% and 21% respectively. The control S_v increased from 21 days to 63 days by 3% and was the maximal out of the four constructs by 63 days. There was a significant difference between the 63 days film and membrane S_v at 63 days (p<0.05). The reaction zone R_{diff} decreased for all four scaffolds from 21 days to 63 days (data not shown). The membrane

had the largest R_{diff} at 63 days while the control had the smallest R_{diff}. There were no significant differences between groups with regards to R_{diff}.

Within the mesh matrix, there was a 7% increase in both L_v and S_v from 21 days to 63 days, while there was a 1% decrease in $R_{diff.}$. None of the changes from 21 days to 63 days were statistically significant.

4. Discussion

The aim of this study was to investigate the cellular and angiogenic *in-vivo* response of a slowly degrading polyesterurethane in a rabbit subcutaneous model at 21 days and 63 days. Three polyesterurethane constructs of different porosity were examined; a non-porous solvent cast film, a porous electrospun mesh and a porous phase inversion membrane. It was hypothesised that scaffold architecture of biodegradable polyesterurethane *in-vivo* evokes a cellular and angiogenic response that is dictated by architecture.

Two distinct zones were evident around the film, membrane and control at both time points. The inner layer, denoted the tissue-implant interface, was densely populated with cell nuclei without much collagenous matter. The outer layer, designated the reaction zone, was more collagenous and interspersed with fibroblasts. These findings concur with Lossing and Hansson who also reported two well-defined layers of a similar nature around silicone implants [22]. The tissue-implant interface thickness was measured at both time points. Stereological analysis quantified the volume fraction of extracellular matrix deposition, inflammatory cells and angiogenesis within the two zones.

The tissue-implant interface is the interfacial region of the inflammatory response induced by an implanted biomaterial *in-vivo*. The tissue-implant interface thickness indicates how well an implanted material is accepted by the host tissue; a large interface would suggest an offending biomaterial. Excessive interface thickness has been suggested as the aetiology of implant failures such as loosening of hip replacements [23,24], blockage of ocular drainage devices for glaucoma [25], malfunctioning of biosensors [26], excessive shrinkage of surgical meshes for hernia repair [27] and post-operative difficulty in removing intravascular pacing leads [28]. In this study, the tissue-implant interface thickness was significantly maximal for the bovine pericardium and minimal for the mesh at both time points.

There are two possible explanations as to why the tissue-implant interface thickness was larger around the bovine pericardium compared to the three polyesterurethane scaffolds, namely biomaterial degradation rate and the by-product of degradation. The polyesterurethane in this study has a degradation rate greater than 12 months [13] while Vaughn and colleagues reported no signs of resorption for bovine pericardium *in-vivo* at 167 days [29]. The latter value would postulate that glutaraldehyde cross-linked bovine pericardium is a slowly degrading material, similar to the polyesterurethane.

The second possible explanation may be the degradation by-products. Cross-linked bovine pericardium has been previously shown to evoke an excessive inflammatory response [30-32]. Previous *in-vitro* analysis of this polyesterurethane indicated that no cytotoxic residues are present on the mesh or film scaffolds post-processing and that both constructs accommodate good cell viability [13]. Furthermore, degradation of the

monomers within this polyesterurethane, namely hydroxybutyrate, glycolide and ε-caprolactone, are all removed via systemic circulation; poly(hydroxybutyrate) degrades into R-3-hydroxybutyric acid which is a natural component of the blood [33], while glycolide is removed via renal excretion [34], as is ε-caprolactone [35].

Although the film and membrane had similar interface thickness at 21 days, the membrane interface thickness increased at 63 days while the film decreased. The irregular surface of the membrane may have caused irritation and inflammation subcutaneously while the rabbits were active. And due to the small pore size of the membrane, 17±7μm, cellular infiltration would not be possible. The lack of cellular infiltration into the membrane may also be attributed to poor pore interconnectivity which would prevent cellular penetration within the membrane. Conversely, there was no tissue-implant interface present around the mesh. This could be explained by the mesh inter-fibre distance, 107±58μm, and pore size, 78±46μm which would accommodate cellular infiltration.

Within the tissue-implant interface, there was no increase in the volume fraction of collagen for the film, with an increase for the membrane. There was an 18% decrease in the volume fraction of collagen around the control. In the reaction zone, there was an increase from 21 days to 63 days in the volume fraction of collagen around all three polyesterurethane scaffolds, while there was a 22% decrease in the volume fraction of collagen for the control. Comparing the 63 days reaction zones of the three polyesterurethane scaffolds, the membrane had the largest volume fraction of collagen, followed by the film and then the mesh.

Picosirius red staining and polarised light microscopy was used to identify collagen fibres around the implants. Under polarised light, yellow and red are thought to signify collagen type I-like fibres, while green suggests collagen type III-like fibres [16-18], the latter indicating active fibrocytes. The presence of the type III-like and type I-like collagen exemplify the transition of fibrocytes to collagen. No collagen was observed within the film, membrane or mesh scaffolds at either time point which correlates with the stereological quantification of the Masson's trichrome-stained slides. There was an even distribution of type I-like and type III-like collagen fibres around the film, membrane and mesh tissue-implant interface at 21 days. At 63 days, the polarised light microscopy images revealed an increase of red and yellow fibres around all implants, which suggests maturation from type III-like collagen. Collagen type I-like and type III-like fibres were observed within the control implants at 21 days and 63 days. This was due to the control material, bovine pericardium, being collagen based.

Within the tissue-implant interface there was an increase in the volume fraction of inflammatory cells for the membrane, film and control from 21 days to 63 days. Further stereological analysis of the inflammatory cells revealed greater quantities of mononuclear cells at both time points for the bovine pericardium compared to the film and membrane scaffolds. In addition, there were larger quantities of lymphocytes contained within the control tissue-implant interface, compared to the film and membrane, at 63 days. The presence of the sustained macrophage response and larger volume fraction of lymphocytes indicate a chronic wound healing response to the bovine pericardium. Almost 40% of the inflammatory cells present within the tissue-implant interface around the film and membrane were fibroblasts. This quantity of fibroblasts is

encouraging as during the wound healing response, granulation tissue is replaced by connective tissue. Hence, the degrading film and membrane scaffolds will be replaced at the same rate with native tissue and without excessive chronic inflammation, as seen with the bovine pericardium.

Stereological analysis indicated greater foreign body giant cells within the porous membrane tissue-implant interface compared to the non-porous film or control. This difference indicates that scaffold **architecture** influences foreign body reaction. However, it is not uncommon for foreign body giant cells to form around porous inert materials who have an irregular morphology with a pore size less than 20µm [4,6,36]. Tienen et al proffered that if inflammatory cells are unable to penetrate small pores then giant cells will accumulate and attempt to phagocytose the material [37].

Quantification of the inflammatory cells indicated that the control reaction zone had at least a factor three times more lymphocytes than the film, mesh and membrane. The reaction zone in the control had a sustained mononuclear cell presence, which along with the lymphocytes, suggest a chronic inflammatory response to the bovine pericardium. There was a significantly greater volume fraction of fibrocytes for the control compared to the three polyesterurethane scaffolds at 63 days, (p<0.05). Fibrocytes are mature fibroblasts that produce collagen type I, collagen type III and fibronectin [38-40]. The presence of fibrocytes around an implanted material also suggest that the scaffold is isolated from the surrounding tissue [41-43].

The three polyesterurethane scaffolds had similar volume fractions of inflammatory cells at 63 days. The non-porous film also had the greater volume fraction of fibroblasts compared to the porous membrane and mesh at 63 days. This may be due

to the non-porous film preventing penetration of fibroblasts, unlike the mesh and membrane, whose interconnecting pores provide a network for the fibroblasts to penetrate. There was no significant difference in the volume fraction of fibrocytes around the mesh, membrane or film. However, the non-porous film had a smaller mean volume fraction of fibrocytes at 63 days compared to the mesh and membrane. This infers that porous scaffolds are better tolerated *in-vivo* compared to non-porous scaffolds. There were mononuclear cells present within the membrane reaction zone, with negligible quantities for the film and mesh. This sustained chronic inflammatory response may be due to the irregular topography of the membrane [4-6].

Examination of the mesh scaffold indicted that there was a 17% decrease in the volume fraction of polymer from 21 days to 63 days. *In-vitro*, the mesh experienced a 33% decrease in molecular weight for the same time period [13]. Although it is not possible to directly compare these two values, this difference can be attributed to the different degradation mechanisms; hydrolytic *in-vitro* compared to hydrolytic and enzymatic *in-vivo*. The volume fraction of inflammatory cells within the mesh interstices decreased by 27% from 21 days to 63 days, with a 129% increase in the volume fraction of fibroblasts and a 56% decrease in the volume fraction of mononuclear cells, ($p<0.05$). The summation of these results denotes that the slowly degrading mesh was well tolerated *in-vivo* and replaced by host tissue.

The third parameter to be quantified was angiogenesis. Angiogenesis is crucial to the long-term integration and success of degrading implants as capillaries provide a network for providing blood, oxygen and nutrients to the newly formed tissue. CD31 is a specific glycoprotein expressed by vascular endothelial cells, and so can be used to infer

angiogenesis [19,20]. Hence slides were stained with CD31 so as to quantify the degree of angiogenesis around and within the four implants at 21 days and 63 days. Analysis of the S_v at 63 days within the tissue-implant interface suggests that the polyesterurethane scaffolds had superior angiogenesis compared to bovine pericardium. Possibly the excessive inflammatory response from the bovine pericardium would prevent angiogenesis whilst concomitantly evoking a chronic wound healing response.

The non-porous film had a significantly smaller R_{diff}, (p<0.05), while the membrane had a higher L_v and S_v at 63 days. An explanation for these results would be that the non-porous film prevents penetration of capillaries within the scaffold and so the newly formed capillaries would become more densely packed. Conversely, porous scaffolds would encourage greater angiogenesis compared to a non-porous scaffold due to the higher surface area per volume.

Within the reaction zone, all polyesterurethane scaffolds recorded a decrease in L_v and S_v. This was contrary to an increase in L_v and S_v within the bovine pericardium reaction zone. The increase in L_v and S_v for the bovine pericardium may be explained by the associated volume fraction increase of fibrocytes, as it has been suggested that fibrocytes induce angiogenesis [38,44].

Out of the three polyesterurethane scaffolds at 63 days, the film had a larger reaction zone L_v and S_v compared to the membrane and mesh. Moreover, the mesh had the smallest R_{diff} out of the three polyesterurethane scaffolds. These results confirm that a porous scaffold is superior to a non-porous scaffold for promoting angiogenesis and that increasing scaffold porosity increases vascularisation. Furthermore, these reported results agree with van Tienen and colleagues who compared the tissue ingrowth of two

polyesterurethane scaffolds with varying porosity [45]. The authors attributed the enhanced fibrovascular ingrowth with increasing scaffold porosity.

Having characterised this slowly degrading polyesterurethane *in-vitro* and *in-vivo*, future research will include functional studies using this material to determine its overall efficacy.

5. Conclusions

This study investigated the *in-vivo* tissue response to a biodegradable polyesterurethane, specifically the cellular and angiogenic response evoked by varying implant architectures in a subcutaneous rabbit implant model. The tissue-implant interface thickness was dependent on the scaffold material and morphology, being minimal for the porous mesh and maximal for the bovine pericardium. All of the polyesterurethane scaffolds showed a significantly less chronic inflammatory reaction than that seen in the control ($p<0.05$). However, the small pore size of the membrane fostered the accumulation of foreign body giant cells. The mesh was the only scaffold infiltrated with host tissue at both time points. Mature collagen was seen around all implants at 63 days. Stereological quantification indicated that all three polyesterurethane scaffolds had superior angiogenesis at both time points compared to the control. Specifically, increasing scaffold porosity promoted superior angiogenesis. Accordingly, it may be concluded that the scaffold architecture of a biodegradable polyesterurethane *in-vivo* evokes a cellular and angiogenic response that is dictated by architecture.

Acknowledgements

The authors would like to thank Marco Camus and Marc Simonet (ETH) for their help with scaffold fabrication. Yolanda Garcia and Ailish Breen (National University of Ireland Galway) for their help with the animal surgery, stereology and cell staining. Sergio Ortega (National University of Ireland Galway) for use of his custom-designed software.

Irish Research Council for Science, Engineering and Technology: funded by the National Development Plan.

Enterprise Ireland: Research Innovation Partnership.

References

1. Riboldi SA, Sampaolesi M, Neuenschwander P, Cossu G, Mantero S. Electrospun degradable polyesterurethane membranes: potential scaffolds for skeletal muscle tissue engineering. Biomaterials 2005;26(22):4606-4615.
2. Guan J, Sacks MS, Beckman EJ, Wagner WR. Synthesis, characterization, and cytocompatibility of elastomeric, biodegradable poly(ester-urethane)ureas based on poly(caprolactone) and putrescine. J Biomed Mater Res 2002;61(3):493-503.
3. Wang JH, Yao CH, Chuang WY, Young TH. Development of biodegradable polyesterurethane membranes with different surface morphologies for the culture of osteoblasts. J Biomed Mater Res 2000;51(4):761-70.
4. Laeschke K. Biocompatibility of microparticles into soft tissue fillers. Semin Cutan Med Surg 2004;23(4):214-217.
5. Salthouse TN. Some aspects of macrophage behavior at the implant interface. J Biomed Mater Res 1984;18(4):395-401.
6. Shun C-T, Young T-H. The effect of surface properties of EVAL membranes on the inflammatory response. Materials Science and Engineering: C 2000;13(1-2):75-83.
7. Sanders JE, Lamont SE, Karchin A, Golledge SL, Ratner BD. Fibro-porous meshes made from polyurethane micro-fibers: effects of surface charge on tissue response. Biomaterials 2005;26(7):813-818.

8. Sanders JE, Bale SD, Neumann T. Tissue response to microfibers of different polymers: polyester, polyethylene, polylactic acid, and polyurethane. J Biomed Mater Res 2002;62(2):222-227.

9. Sanders JE, Lamont SE, Mitchell SB, Malcolm SG. Small fiber diameter fibro-porous meshes: tissue response sensitivity to fiber spacing. J Biomed Mater Res A 2005;72(3):335-342.

10. Saad B, Ciardelli G, Matter S, Welti M, Uhlschmid GK, Neuenschwander P, Suter UW. Characterization of the cell response of cultured macrophages and fibroblasts to particles of short-chain poly[(R)-3-hydroxybutyric acid]. J Biomed Mater Res 1996;30(4):429-429.

11. Saad B, Hirt TD, Welti M, Uhlschmid GK, Neuenschwander P, Suter UW. Development of degradable polyesterurethanes for medical applications: in vitro and in vivo evaluations. J Biomed Mater Res 1997;36(1):65-74.

12. Kylma J, Seppälä JV. Synthesis and Characterization of a Biodegradable Thermoplastic Poly(ester-urethane) Elastomer. Macromolecules 1997;30:2876-2882.

13. Henry JA, Simonet M, Pandit A, Neuenschwander P. Characterization of a slowly degrading biodegradable polyester-urethane for tissue engineering scaffolds. J Biomed Mater Res 2007;82A(3):669-79.

14. Saad B, Keiser OM, Welti M, Uhlschmid GK, Neuenschwander P, Suter UW. Multiblock copolyesters as biomaterials: in vitro biocompatibility testing. J Mater Sci Mater Med 1997;8(8):497-505.

15. Saad B, Neuenschwander P, Uhlschmid GK, Suter UW. New versatile, elastomeric, degradable polymeric materials for medicine. Int J Biol Macromol 1999;25(1-3):293-301.

16. Cuttle L, Nataatmadja M, Fraser JF, Kempf M, Kimble RM, Hayes MT. Collagen in the scarless fetal skin wound: detection with picrosirius-polarization. Wound Repair Regen 2005;13(2):198-204.

17. Madibally SV, Solomon V, Mitchell RN, Van De Water L, Yarmush ML, Toner M. Influence of insulin therapy on burn wound healing in rats. J Surg Res 2003;109(2):92-100.

18. Zhang H, Sun L, Wang W, Ma X. Quantitative analysis of fibrosis formation on the microcapsule surface with the use of picro-sirius red staining, polarized light microscopy, and digital image analysis. J Biomed Mater Res 2006;76A(1):120-125.

19. Walles T, Herden T, Haverich A, Mertsching H. Influence of scaffold thickness and scaffold composition on bioartificial graft survival. Biomaterials 2003;24(7):1233-1239.

20. Henno S, Lambotte JC, Glez D, Guigand M, Lancien G, Cathelineau G. Characterisation and quantification of angiogenesis in beta-tricalcium phosphate implants by immunohistochemistry and transmission electron microscopy. Biomaterials 2003;24(19):3173-3181.

21. Garcia Y, Breen A, Burugapalli K, Dockery P, Pandit A. Stereological methods to assess tissue response for tissue-engineered scaffolds. Biomaterials 2007;28(2):175-186.

22. Lossing C, Hansson HA. Peptide growth factors and myofibroblasts in capsules around human breast implants. Plast Reconstr Surg 1993;91(7):1277-1286.

23. Bader R, Mittelmeier W, Zeiler G, Tokar I, Steinhauser E, Schuh A. Pitfalls in the use of acetabular reinforcement rings in total hip revision. Arch Orthop Trauma Surg 2005;125(8):558-563.

24. Davies AP, Willert HG, Campbell PA, Learmonth ID, Case CP. An unusual lymphocytic perivascular infiltration in tissues around contemporary metal-on-metal joint replacements. J Bone Joint Surg Am 2005;87(1):18-27.

25. Kivalo M, Siren V, Raitta C, Immonen I. Biodegradable tube implants in experimental glaucoma surgery in the rabbit. J Mater Sci Mater Med 1999;10(1):53-58.

26. Chen HC, Ahmed J. Design and testing of a fluorescence glucose sensor which incorporates a bioinductive material. Biomed Sci Instrum 2004;40:149-154.

27. Schumpelick V, Conze J, Klinge U. Preperitoneal mesh-plasty in incisional hernia repair. A comparative retrospective study of 272 operated incisional hernias. Chirurg 1996;67(10):1028-1035.

28. Smith HJ, Fearnot NE, Byrd CL, Wilkoff BL, Love CJ, Sellers TD. Five-years experience with intravascular lead extraction. U.S. Lead Extraction Database. Pacing Clin Electrophysiol 1994;17(11 Pt 2):2016-2020.

29. Vaughn CC, Vaughn PL, Vaughn CC, 3rd, Sawyer P, Manning M, Anderson D, Roseman L, Herbst TJ. Tissue response to biomaterials used for staple-line reinforcement in lung resection: a comparison between expanded

polytetrafluoroethylene and bovine pericardium. Eur J Cardiothorac Surg 1998;13(3):259-265.

30. Bullaboy CA. Bovine pericardium: another cautionary note. Ann Thorac Surg 1989;48(5):743.

31. Grabenwoger M, Sider J, Fitzal F, Zelenka C, Windberger U, Grimm M, Moritz A, Bock P, Wolner E. Impact of glutaraldehyde on calcification of pericardial bioprosthetic heart valve material. Ann Thorac Surg 1996;62(3):772-777.

32. Dahn M, Lyman WD, Schwell AB, Factor SM, Frater RW. Immunogenicity of glutaraldehyde-tanned bovine pericardium. J Thorac Cardiovasc Surg 1990;111:1082-1090.

33. Zinn M, Witholt B, Egli T. Occurrence, synthesis and medical application of bacterial polyhydroxyalkanoate. Adv Drug Deliv Rev 2001;53(1):5-21.

34. Gunatillake P, Mayadunne R, Adhikari R. Recent developments in biodegradable synthetic polymers. Biotechnol Annu Rev 2006;12:301-347.

35. Webb AR, Yang J, Ameer GA. Biodegradable polyester elastomers in tissue engineering. Expert Opin Biol Ther 2004;4(6):801-812.

36. Woodward S. Evaluation by light microscopy. Philadelphia: Taylor & Francis; 1999. pp 599-611

37. van Tienen T, Heijkants RG, de Groot JH, Schouten AJ, Pennings AJ, Veth RP, Buma P. Meniscal replacement in dogs. Tissue regeneration in two different materials with similar properties. J Biomed Mater Res B Appl Biomater 2006;76(2):389-396.

38. Quan TE, Cowper S, Wu SP, Bockenstedt LK, Bucala R. Circulating fibrocytes: collagen-secreting cells of the peripheral blood. Int J Biochem Cell Biol 2004;36(4):598-606.

39. Bucala R, Spiegel LA, Chesney J, Hogan M, Cerami A. Circulating fibrocytes define a new leukocyte subpopulation that mediates tissue repair. Mol Med 1994;1(1):71-81.

40. Abe R, Donnelly SC, Peng T, Bucala R, Metz CN. Peripheral blood fibrocytes: differentiation pathway and migration to wound sites. J Immunol 2001;166(12):7556-62.

41. Therin M, Christel P, Meunier A. Analysis of the general features of the soft tissue response to some metals and ceramics using quantitative histomorphometry. J Biomed Mater Res 1994;28(11):1267-76.

42. Takeshita F, Morimoto K, Suetsugu T. Tissue reaction to alumina implants inserted into the tibiae of rats. J Biomed Mater Res 1993;27(4):421-8.

43. Ye Q, Ohsaki K, Ii K, Li DJ, Zhu CS, Yamashita Y, Tenshin S, Takano-Yamamoto T. Subcutaneous inflammatory reaction to a synthetic auditory ossicle (Bioceram) in rats. Acta Otolaryngol 1999;119(1):83-8.

44. Hartlapp I, Abe R, Saeed RW, Peng T, Voelter W, Bucala R, Metz CN. Fibrocytes induce an angiogenic phenotype in cultured endothelial cells and promote angiogenesis in vivo. Faseb J 2001;15(12):2215-24.

45. van Tienen TG, Heijkants RGJC, Buma P, de Groot JH, Pennings AJ, Veth RPH. Tissue ingrowth and degradation of two biodegradable porous polymers with different porosities and pore sizes. Biomaterials 2002;23(8):1731-1738.

Figure Legends

Figure 1 – SEM images of processed polyesterurethane variants (a) solvent cast film (b) phase inversion membrane and (c) electrospun mesh

Figure 2 – H&E histological images (original magnification x10) illustrating the tissue response elicited by: (a, b) non-porous film, (c, d) porous membrane, (e, f) control and (g, h) porous mesh, at 21 days (a, c, e, g) and 63 days (b, d, f, h) in a subcutaneous rabbit model. White arrowheads indicate tissue-implant interface, black arrows indicate reaction zone

Figure 3 – (a) Stereological volume fraction analysis of the Masson's trichrome slides, describing the tissue-implant interface for the film, membrane and control, at 21 days and 63 days (b) Stereological volume fraction analysis of the of the Masson's trichrome slides for reaction zone of the mesh, film, membrane and control, at 21 days and 63 days (c) Stereological volume fraction analysis of the 21 days and 63 days tissue infiltration for the mesh. All values expressed as mean ± SD. *, # indicates statistical difference, $p<0.05$, between groups

Figure 4 – Polarised light microscopy images (original magnification x40) of (a, b) film, (c, d) membrane, (e, f) mesh and (g, h) control, at 21days (a, c, e, g) and 63 days (b, d, f, h) in a subcutaneous rabbit model. Yellow and red denote collagen type I-like tissue whilst green implies collagen type III-like tissue. Arrows indicate interface tissue-implant interface

Figure 5 – (a) Stereological volume fraction analysis of the 21 days and 63 days inflammatory response within the film, membrane and control tissue-implant interface (b) Stereological volume fraction analysis of the 21 days and 63 days inflammatory response within the mesh, film, membrane and control reaction zone (c) Stereological volume fraction analysis of the 21 days and 63 days inflammatory response within the mesh matrix. F = fibroblasts, GC = giant cells, L = lymphocytes, P = plasma cells, MN = mononuclear cells. All values expressed as mean ± SD. Identical letters indicate statistical difference, $p<0.05$, between groups

Figure 6 – Light microscopy images (original magnification x40) of CD31 immunostained slides of (a) film, (b) membrane (c) mesh and (d) control at 21d in a subcutaneous rabbit model. Arrows indicate blood vessels as detected by CD31 labelled endothelial cells

Figure 7 – (a) Tissue-implant interface surface area density, S_v, of the membrane, film and control at 21 and 63 days (b) Tissue-implant interface radial diffusion difference, R_{diff}, of the membrane, film and control at 21 and 63 days. All values expressed as mean ± SD. * indicates statistical difference, $p<0.05$**,** between groups

Figure 8 – Reaction zone surface area density, S_a, of the membrane, film, mesh and control at 21 and 63 days. All values expressed as mean ± SD. * indicates statistical difference, $p<0.05$, between groups

Parameter	Value
Porosity	91.67 ± 3.51%
Pore size	78.23 ± 45.69µm
Pore distribution:	
aspect ratio 1.0	0.03 ± 0.01
aspect ratio 1.5	0.03 ± 0.01
aspect ratio 2.0	0.03 ± 0.00

Table 1 – Electrospun mesh parameters, mean ± SD, quantified using FFT algorithms

Variant	21 days interface thickness (µm)	63 days interface thickness (µm)
Mesh	0#	0#
Membrane	9 ± 3	14 ± 5
Film	9 ± 4	9 ± 3
Control	14 ± 4*	20 ± 9

Table 2 – Tissue-implant interface thickness, mean ± SD, quantified at 21 and 63 days. *, # denotes statistical difference, $p<0.05$

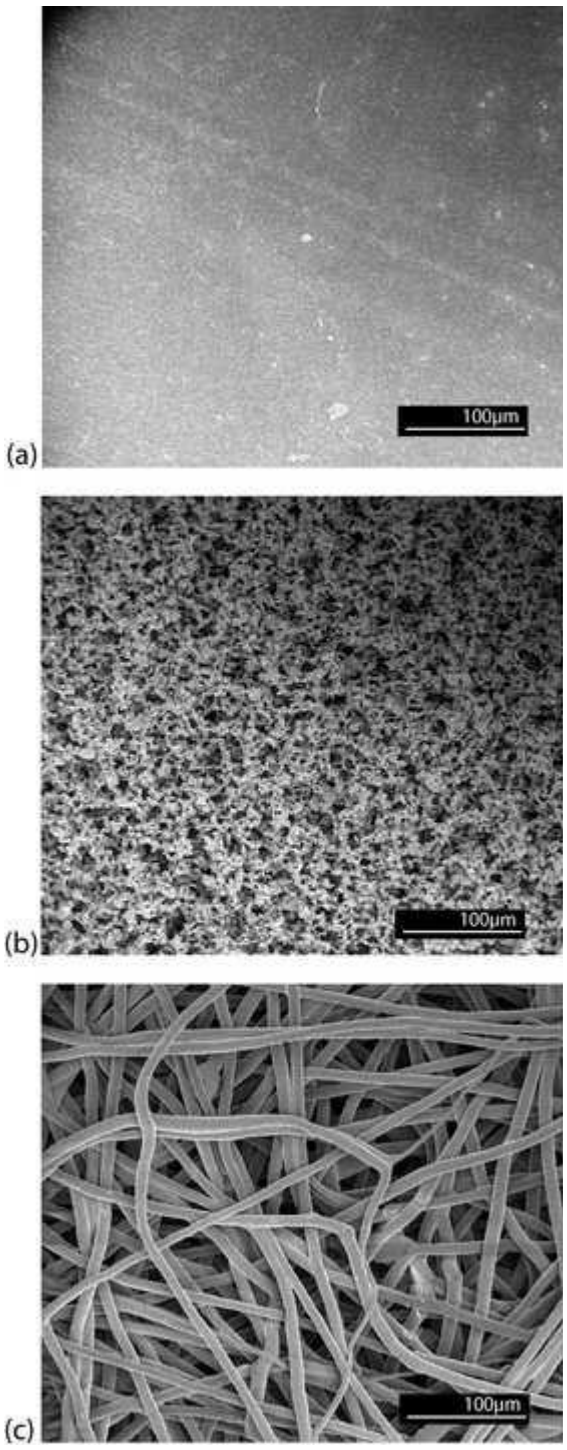

Figure 1

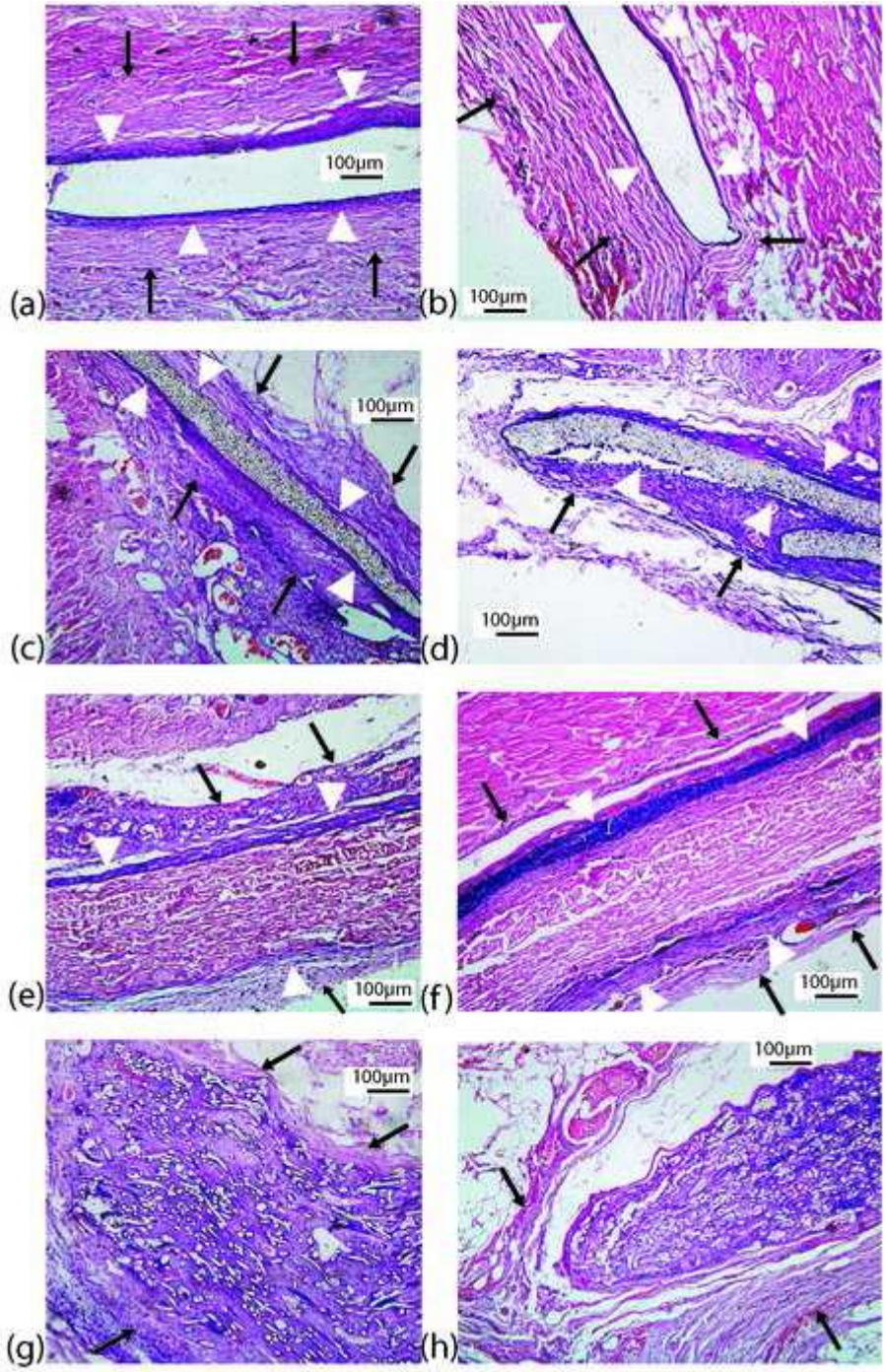

Figure 2

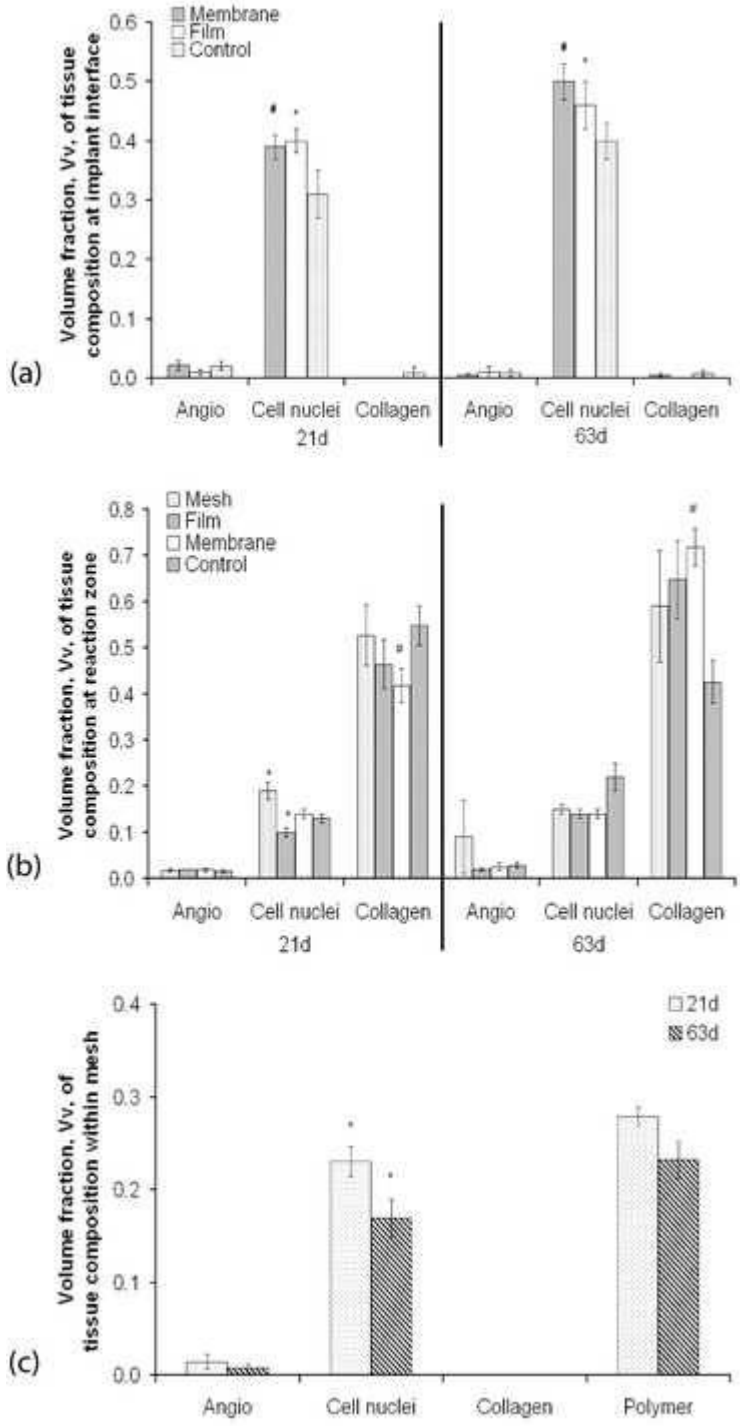
(a)
Membrane
Film
Control
Volume fraction, Vv, of tissue composition at implant interface
0.6
0.5
0.4
0.3
0.2
0.1
0.0
Angio
Cell nuclei
Collagen
21d
63d
(b)
Mesh
Film
Membrane
Control
Volume fraction, Vv, of tissue composition at reaction zone
0.8
0.7
0.6
0.5
0.4
0.3
0.2
0.1
0.0
(c)
21d
63d
Volume fraction, Vv, of tissue composition within mesh
0.4
0.3
0.2
0.1
0.0
Polymer

Figure 3

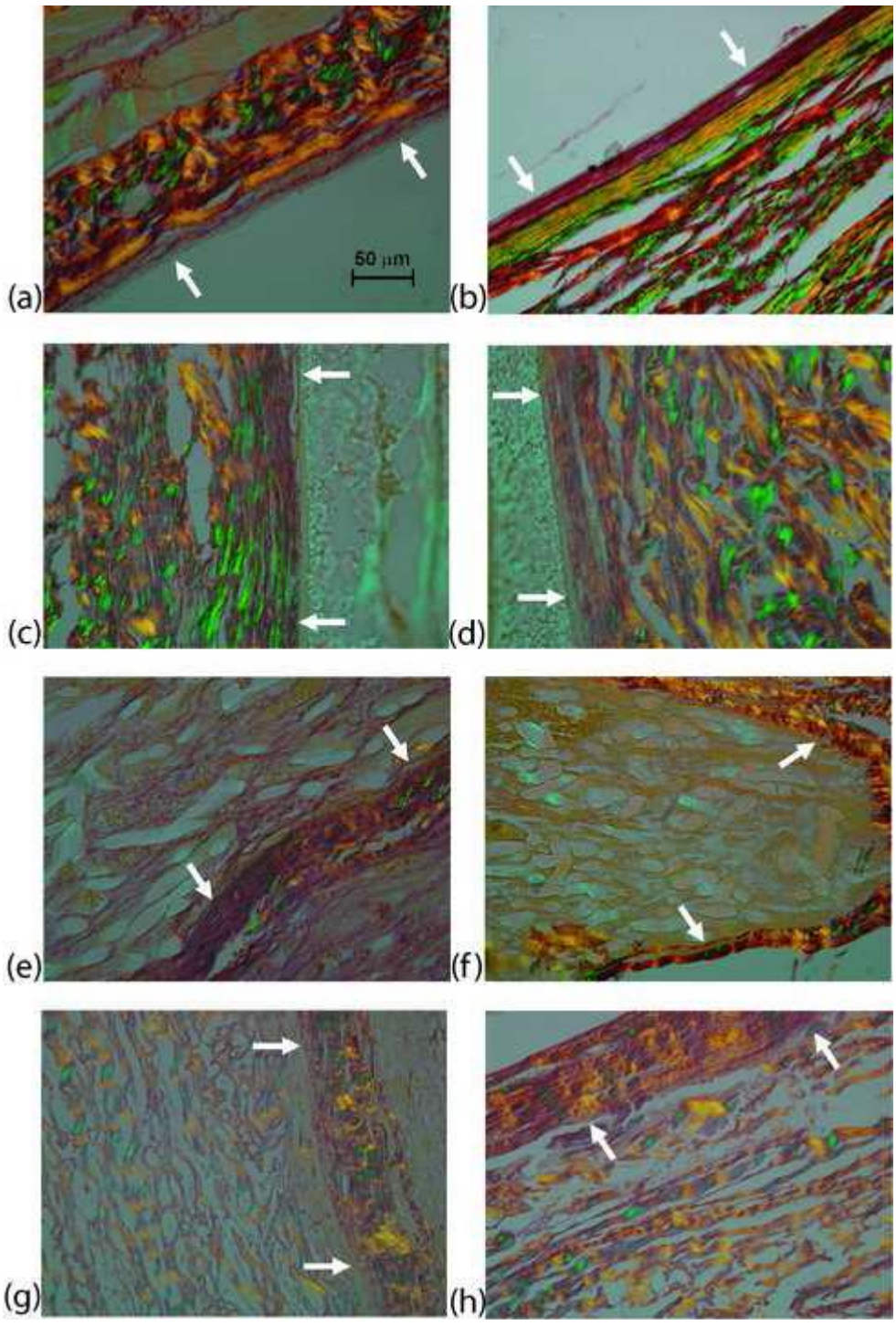

Figure 4

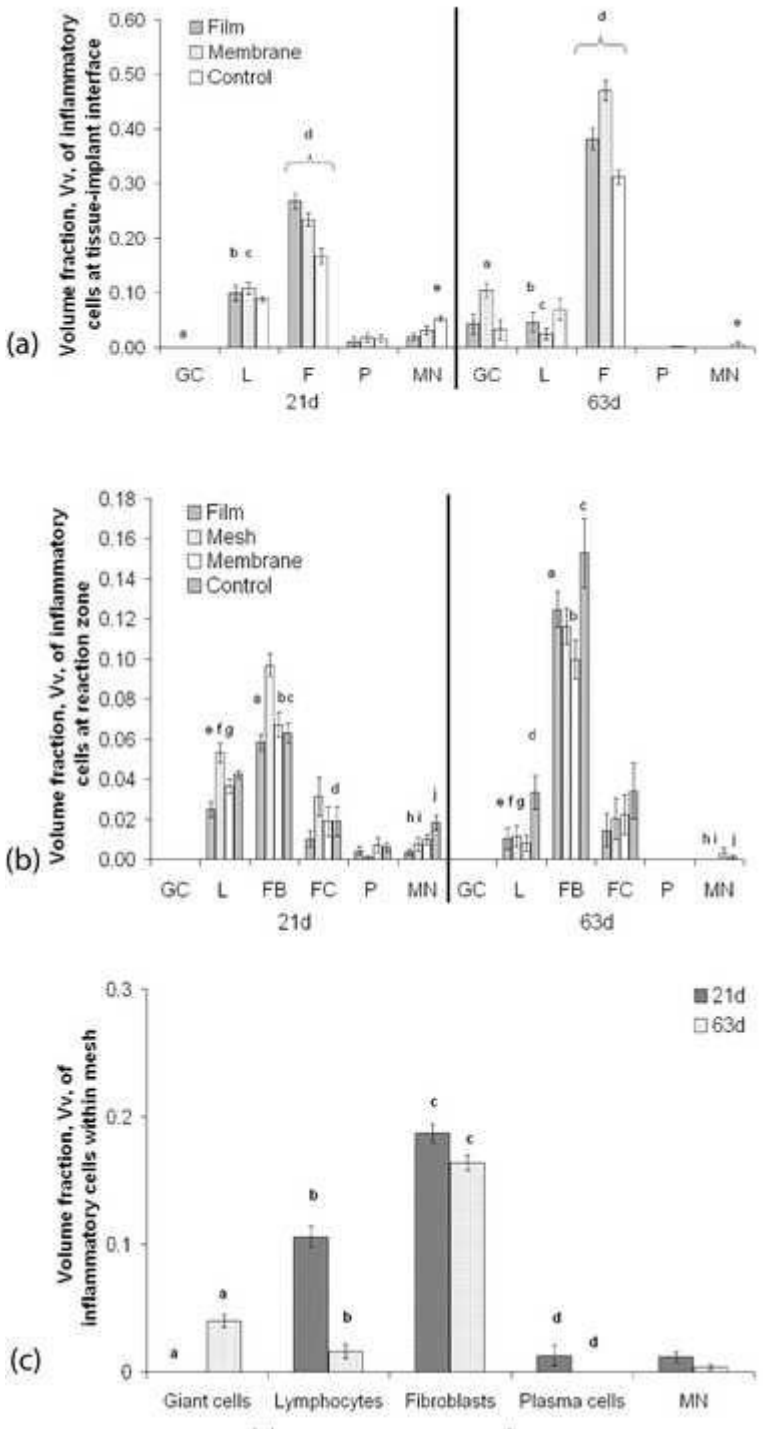
(a)
Volume fraction, Vv, of inflammatory cells at tissue-implant interface
Film
Membrane
Control
GC
L
F
P
MN
21d
63d
(b)
Volume fraction, Vv, of inflammatory cells at reaction zone
Film
Mesh
Membrane
Control
GC
L
FB
FC
P
MN
21d
63d
(c)
Volume fraction, Vv, of inflammatory cells within mesh
21d
63d
Giant cells
Lymphocytes
Fibroblasts
Plasma cells
MN

Figure 5

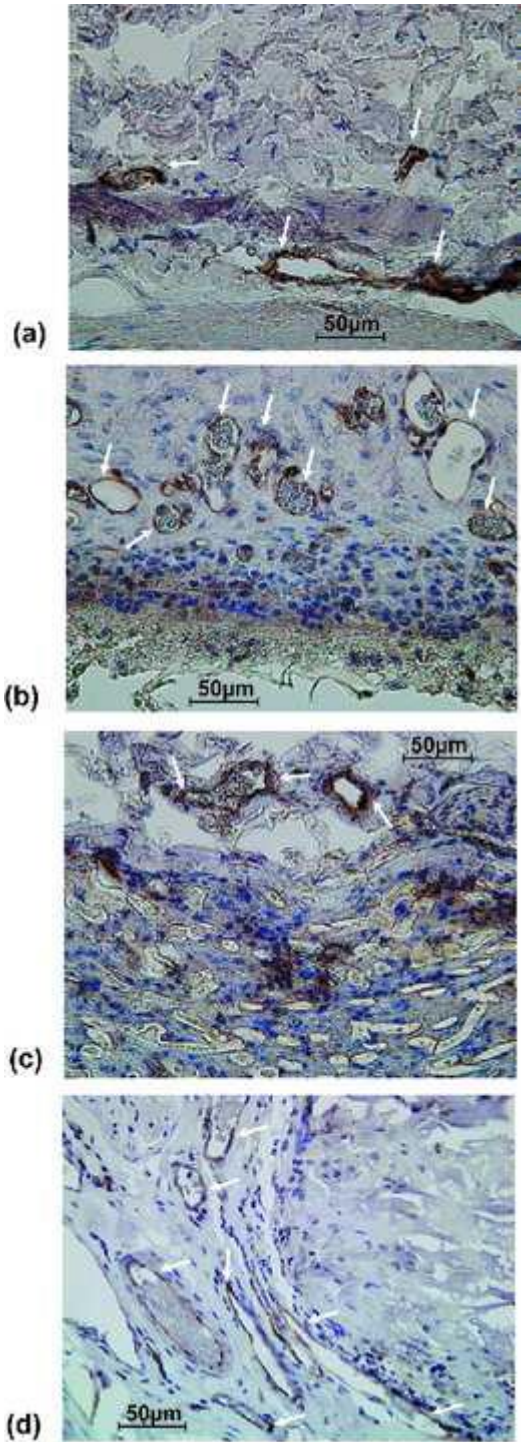

Figure 6

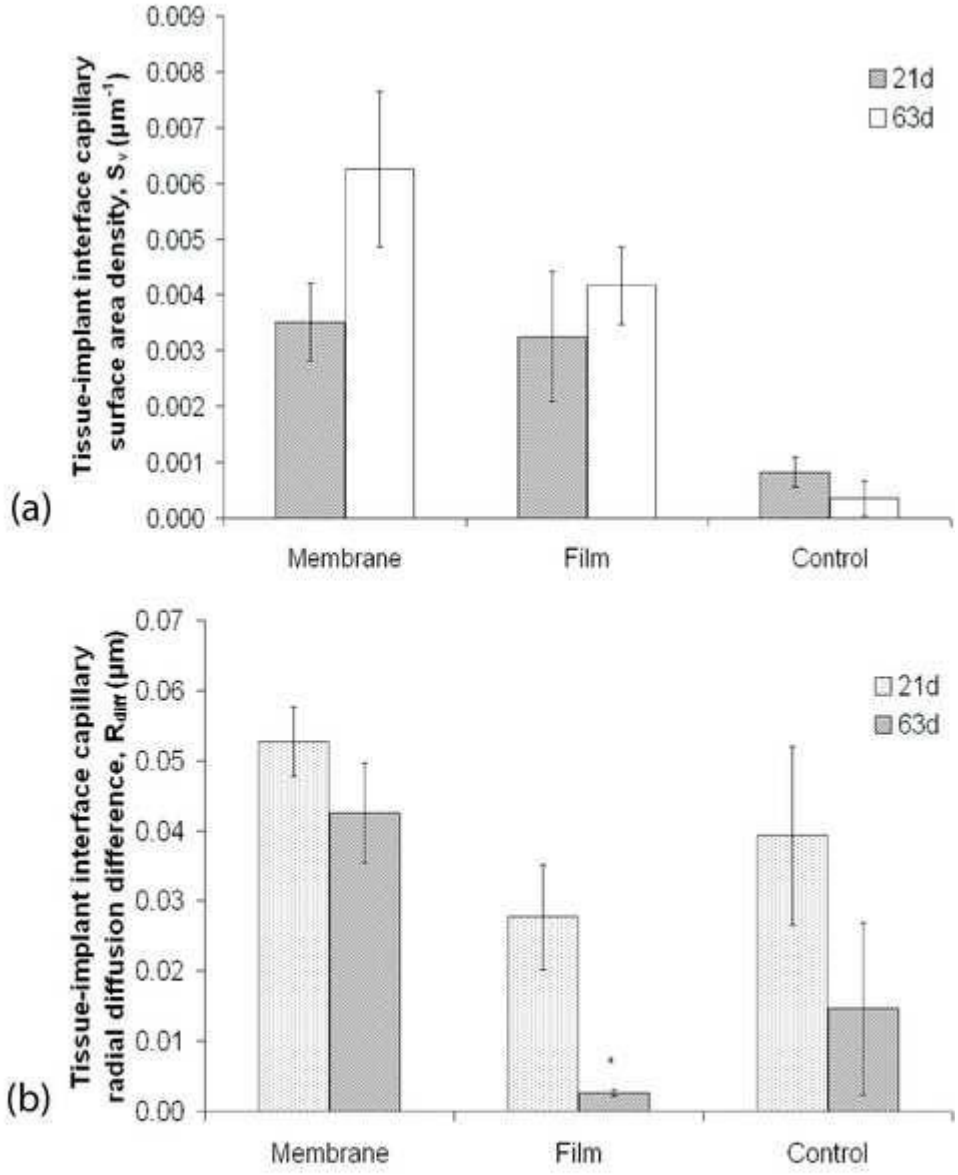
(a)
Tissue-implant interface capillary surface area density, S_v (μm^{-1})
0.009
0.008
0.007
0.006
0.005
0.004
0.003
0.002
0.001
0.000
21d
63d
Membrane
Film
Control
(b)
Tissue-implant interface capillary radial diffusion difference, R_{diff} (µm)
0.07
0.06
0.05
0.04
0.03
0.02
0.01
0.00
21d
63d
Membrane
Film
Control

Figure 7

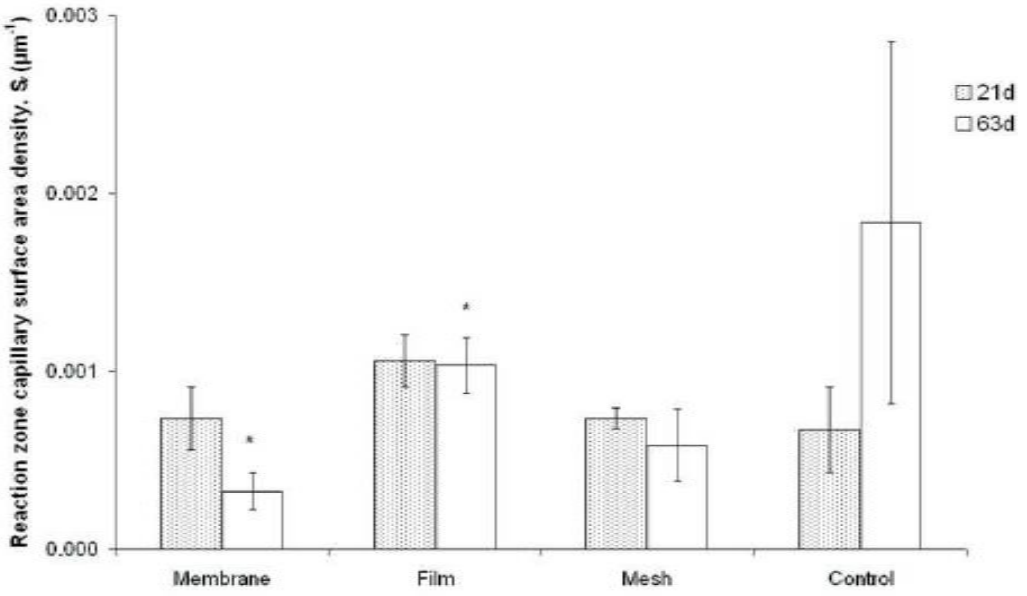
Reaction zone capillary surface area density, S (µm-1)
0.003
0.002
0.001
0.000
21d
63d
*
*
Membrane
Film
Mesh
Control

Figure 8